

Analysis of the HO₂ Vibrational Spectrum on an Accurate Ab Initio Potential Energy Surface[†]

Chuanxiu Xu, Bin Jiang, and Daiqian Xie*

Institute of Theoretical and Computational Chemistry, Key Laboratory of Mesoscopic Chemistry, School of Chemistry and Chemical Engineering, Nanjing University, Nanjing 210093, People's Republic of China

Stavros C. Farantos*

Institute of Electronic Structure and Laser, Foundation for Research and Technology-Hellas, Iraklion 71110, Crete, Greece, and Department of Chemistry, University of Crete, Iraklion, Crete, Greece

Shi Ying Lin and Hua Guo*

Department of Chemistry and Chemical Biology, University of New Mexico, Albuquerque, New Mexico 87131

Received: March 23, 2007; In Final Form: May 18, 2007

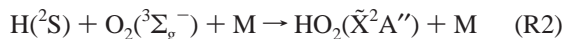
The complete vibrational spectrum of the HO₂(\tilde{X}^2A'') radical, up to the H + O₂ dissociation limit, has been determined quantum mechanically on an accurate potential energy surface (PES), based on ~15000 ab initio points at the icMRCI+Q/aug-cc-pVQZ level of theory. The vibrational states are found to be assignable at low energies but become more irregular as the energy approaches the dissociation limit. However, even at very high energies, regularity still exists, in sharp contrast to earlier results based on the double many-body expansion (DMBE) IV potential. Several Fermi resonances have been identified, and the spectrum is fit with a spectroscopic Hamiltonian. In addition, the vibrational dynamics is analyzed using a periodic orbit approach.

I. Introduction

The hydroperoxyl radical (HO₂) is an important intermediate species in combustion processes. Indeed, the following endothermic reaction is the bottleneck in the combustion of hydrogen and hydrocarbons:¹

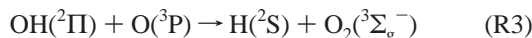


It proceeds on the potential of the ground electronic state HO₂(\tilde{X}^2A''), and is strongly influenced by the long-lived resonances supported by the deep HO₂ well (~2.3 eV to the H + O₂ limit). Under combustion conditions, the transient HO₂ complex may be stabilized by a third body in the following recombination reaction:¹



thus competing with reaction R1.

The reverse reaction of reaction R1, namely,



is known to have an important role in interstellar chemistry at low temperatures,² thanks to the barrierless nature of this radical–radical reaction and the long-range interactions between the reactants. In addition, HO₂ is also a key species in many atmospheric processes,³ including ozone destruction.⁴

The aforementioned chemical processes underline the importance of the HO₂ system, which has been subjected to many experimental and theoretical studies. (For a recent review, see ref 5.) We note that most of our current theoretical understanding of this system has been derived from a popular semiempirical potential energy surface (PES) developed by Varandas and his co-workers.⁶ In particular, extensive quantum calculations of the HO₂ vibrational spectrum have been reported on this PES.^{7–15} This so-called double many-body expansion (DMBE) IV PES was constructed more than 15 years ago from limited ab initio points and available experimental information. While it provided the best global PES at that time, it contains significant inaccuracies.^{16–18} In particular, the DMBE IV PES substantially underestimates fundamental vibrational frequencies of the HO₂ species. As a result, the highly excited vibrational states of HO₂ were found to be completely irregular and unassignable.^{8–10} Chaotic dynamics was also observed in classical trajectory studies on the same PES.¹⁹ Indeed, dynamic studies on the DMBE IV PES have led Schinke et al.²⁰ to the conclusion that HO₂ represents a prototypical triatomic system with strong intramolecular energy redistribution.

Recently, Xu, Xie, Zhang, Lin, and Guo (XXZLG) reported a new PES for HO₂(\tilde{X}^2A''), based on ~15000 symmetry unique ab initio points using the internally contracted multireference configuration interaction method with the Davidson correction (icMRCI+Q) and the aug-cc-pVQZ basis set.²¹ These ab initio points span a large configuration space, and they were fit using a three-dimensional cubic spline method. (Very recently, the ab initio data set has been updated with better convergent results and fit to analytic forms.²²) It was shown that the new PES provides a much better agreement with experimental vibrational band origins, reducing the errors in the fundamental frequencies

* Authors to whom correspondence should be addressed. Tel.: 505 277 1716. Fax: 505 277 2609. E-mail address: hguo@unm.edu. E-mail: dqxie@nju.edu.cn. E-mail: farantos@iesl.forth.gr.

[†] Part of the special issue “Robert E. Wyatt Festschrift”.

to a few wavenumbers.²¹ In a preliminary report, we have illustrated that the vibrational spectrum of HO₂ is not completely irregular: many highly excited levels are assignable.²³ This observation is in sharp contrast to the earlier conclusion concerning the vibrational dynamics of HO₂²⁰ and may also have important implications for reactions R1–R3.²⁴ In this publication, we provide details of our quantum calculations and additional results on the vibrational dynamics on the updated XXZLG PES. In addition, further insights were gained by a periodic orbit analysis of the excited vibrational dynamics. This paper is organized as follows. The computational details are given in section II, the results are presented and discussed in section III, and the conclusions are given in section IV.

II. Computational Details

A. Lanczos Method. The traditional approach for diagonalizing the Hamiltonian matrix (**H**) is based on the Householder method,²⁵ which yields the complete list of eigenvalues and eigenfunctions. However, this robust and accurate method becomes inadequate when the dimension of the matrix (*N*) increases beyond 10 000, because of unfavorable scaling laws in both arithmetic operations and memory. A useful alternative to this direct diagonalization approach is recursive methods based on Krylov subspaces,²⁶ such as that suggested by Lanczos.²⁷ The basic idea is to recursively generate a small number of vectors that span the eigenspace of interest, rendering a relatively easy diagonalization of a smaller and/or more-sparse matrix. Because of the recursive nature, these methods typically have more favorable scaling laws.

In the Lanczos method,²⁷ the Lanczos vector is updated by the following three-term recursion formula:

$$\mathbf{q}_{k+1} = \beta_k^{-1}[(\mathbf{H} - \alpha_k)\mathbf{q}_k - \beta_{k-1}\mathbf{q}_{k-1}] \quad (\text{for } k = 1, 2, \dots) \quad (1)$$

Each step of the recursion yields two scalar quantities:

$$\alpha_k = \mathbf{q}_k^T(\mathbf{H}\mathbf{q}_k - \beta_{k-1}\mathbf{q}_{k-1}) \quad (2)$$

$$\beta_k = \|(\mathbf{H} - \alpha_k)\mathbf{q}_k - \beta_{k-1}\mathbf{q}_{k-1}\| \quad (\beta_0 = 0) \quad (3)$$

which form the tridiagonal Lanczos matrix:

$$\mathbf{T}^{(K)} = \begin{pmatrix} \alpha_1 & \beta_1 & \cdots & 0 \\ \beta_1 & \alpha_2 & \beta_2 & \vdots \\ & \beta_2 & \ddots & \beta_{K-1} \\ 0 & \vdots & \beta_{K-1} & \alpha_K \end{pmatrix} \quad (4)$$

The diagonalization of the tridiagonal Lanczos matrix, which is relatively straightforward, yields the approximate eigenvalues. In some cases, the eigenfunctions are needed. They can be obtained using an additional Lanczos recursion with the eigenvectors determined in the first recursion. An interesting observation is that the eigenvalues near the spectral extrema converge relatively quickly, when $K \ll N$. As a result, the Lanczos method is particularly efficient for low-lying eigenvalues. The Lanczos method requires only two vectors to be stored in the fast memory, because only the action of the Hamiltonian must be computed. The latter operation relies on matrix-vector multiplication, which is particularly advantageous if the matrix is sparse or factorizable. For these reasons, the Lanczos method is ideally suited for large dimensional problems such as the one studied here.

Although the Lanczos method has been in existence for more than half a century, its applications in molecular physics have been limited until quite recently. Wyatt was among the first to popularize the recursive approach,^{28–30} which has flourished to become the method of choice today for studying highly excited vibrational spectra.^{31,32} In particular, he promoted the approach of Cullum and Willoughby for identifying the so-called spurious eigenvalues that emerge in finite-precision arithmetic without the expensive orthogonalization,³³ which renders the implementation of the Lanczos diagonalizer straightforward and very efficient. Our implementation of the Lanczos method has been reviewed in refs 32 and 34, so no more detail is given here.

B. Hamiltonian and Discretization. The $J = 0$ Hamiltonian is given in the H + O₂ Jacobi coordinates:

$$\hat{H} = -\frac{1}{2\mu_R} \frac{\partial^2}{\partial R^2} - \frac{1}{2\mu_r} \frac{\partial^2}{\partial r^2} + \left(\frac{1}{2\mu_R R^2} + \frac{1}{2\mu_r r^2} \right) \hat{j}^2 + V(R, r, \gamma) \quad (5)$$

where R is the distance from H to the center of mass of the O₂ moiety, r the internuclear distance of O–O, and γ the angle between R and r . The choice of the coordinates allows symmetry adaptation, with respect to the exchange of the two O atoms. \hat{j}^2 is the angular momentum operator, and μ_R and μ_r are the reduced masses of H–O₂ and O₂, respectively. $V(R, r, \gamma)$ is the PES. In this work, we used the spline fit of the modified XXZLG data set.²²

The Hamiltonian was discretized with a direct product basis, which consists of sinusoidal discrete variable representations (DVRs) for the radial Jacobi coordinates and a finite basis representation (FBR) for the angular variable.³⁵ The matrix representation of the radial kinetic energy operator in the DVR is well-known,³⁶ and the angular kinetic energy operator is diagonal in the FBR that is composed of Legendre polynomials. The potential energy operator is diagonal in a grid, which can be reached by a pseudo-spectral transform from the angular coordinate.³⁷ Such a direct product structure allows the factorization of the Hamiltonian matrix, facilitating efficient evaluation of its action onto the Lanczos vector in eq 1.

C. Assignment and Spectroscopic Hamiltonian. The low-lying eigenvalues of the Hamiltonian are mostly assignable with three quantum numbers (n_1, n_2, n_3), which represent the O–H stretching, H–O–O bending, and O–O stretching modes, respectively. The assignment was made with the help of mean square displacements:

$$\langle d^2 \rangle = \langle n | (q - q_e)^2 | n \rangle \quad (6)$$

in which $q = R_{\text{O–H}}, R_{\text{O–O}},$ or $\cos\theta_{\text{H–O–O}}$, and q_e is the corresponding equilibrium value. As we have shown earlier, $\langle d^2 \rangle$ can be readily obtained with a Lanczos-based perturbation method.³⁸ In many cases, the nodal structure of the eigenfunction must be used to confirm the assignment, especially when significant mode mixing occurs.

The 80 lowest assigned eigenvalues were used to construct a spectroscopic Hamiltonian. The diagonal element of the effective Hamiltonian is expressed in a Dunham expansion:

$$\langle n_1, n_2, n_3 | \hat{H} | n_1, n_2, n_3 \rangle = \sum_i \left(n_i + \frac{1}{2} \right) \omega_i + \sum_{i \leq j} \left(n_i + \frac{1}{2} \right) \left(n_j + \frac{1}{2} \right) x_{ij} + \sum_{i \leq j \leq k} \left(n_i + \frac{1}{2} \right) \left(n_j + \frac{1}{2} \right) \left(n_k + \frac{1}{2} \right) y_{ijk} \quad (7)$$

where ω_i is the harmonic frequencies, and the x_{ij} and y_{ijk} are the anharmonicities. We have also included the following off-diagonal elements, because of a Fermi resonance (vide infra):³⁹

$$\langle n_1, n_2, n_3 | \hat{H} | n_1 - 1, n_2 + 1, n_3 + 2 \rangle = \frac{1}{2} \sqrt{n_1(n_2 + 1)(n_3 + 2)(n_3 + 1)} \times [-k + \lambda_1 n_1 + \lambda_2(n_2 + 1) + \lambda_3(n_3 + 2)] \quad (8)$$

The nonlinear fitting was performed using the Powell method.⁴⁰

D. Statistical Analysis. To gauge the extent of regularity in the highly excited region of the HO₂ spectrum, we have analyzed the nearest-neighbor-level spacing (NNLS) distribution and the Δ_3 distribution. The former is defined as $P(s)$ with $s = E_{n+1} - E_n$ and provides an indication of the short-range level repulsion.⁴¹ On the other hand, the latter shed light onto the long-range spectral fluctuations.⁴² Following the procedure of Zimmerman et al.,⁴³ the spectrum was first unfolded to obtain an unbiased average level density. The NNLS and Δ_3 distributions were then computed from the unfolded spectrum.

E. Periodic Orbit Analysis. Details of a vibrational spectrum and its assignment, as well as localization/regularity of the wavefunctions in configuration space can be unraveled by performing a periodic orbit (PO) analysis.^{44–48} Families of stable POs that emanate from a minimum of a potential function can be used to assign overtone states at very high excitation energies. These families are associated with the vibrational normal modes, and they are called principals. Furthermore, bifurcations of POs and the appearance of new families can elucidate observed spectroscopic features that are difficult to extract from the quantum mechanical calculations.⁴⁴

The theory of POs and their bifurcations is now a quite advanced and mature subject.⁴⁹ Locating POs for a molecule is equivalent of finding solutions of Hamilton's equations of motion that satisfy the two-point boundary conditions

$$B[x(0);T] = x(T) - x(0) = 0 \quad (9)$$

where x denotes the vector of all coordinates and their conjugate momenta of nuclei in the molecule, and T the period of the PO. To solve this problem, we use multiple shooting methods, which have been described extensively in previous publications.^{50,51} In this article, we show that localized and assignable high-energy overtone states of the O–O stretch found in the quantum calculations are due to a saddle-node (SN) bifurcation of the principal family.

III. Results

The contour plots of the modified XXZLG PES are displayed in Figure 1 in two sets of coordinates. The PES is dominated by the two equivalent minima, corresponding to two bent HOO isomers ($R = 2.468a_0$, $r = 2.521a_0$, $\theta = 46.18^\circ$ and 133.82°). An immediate observation of the PES is the floppiness of the molecule at moderately high energies, thanks to an isomerization barrier between the two isomers. The tilted potential contours in the lower panel are also indicative of strong coupling between the O–H stretching and the H–O–O bending modes. The HO₂ species dissociates to either the H + O₂ or the HO + O limit, with the latter being 0.536 eV higher than the former.

In our Lanczos calculations, we used 260 (180) equidistant DVR points for the R (r) coordinate from $0.2a_0$ to $10.0a_0$ ($1.0a_0$ to $8.0a_0$). For the angular variable, a 65-point Gauss–Legendre grid was chosen, including only the rotational states corresponding to the odd O–O exchange parity. For low-lying energy

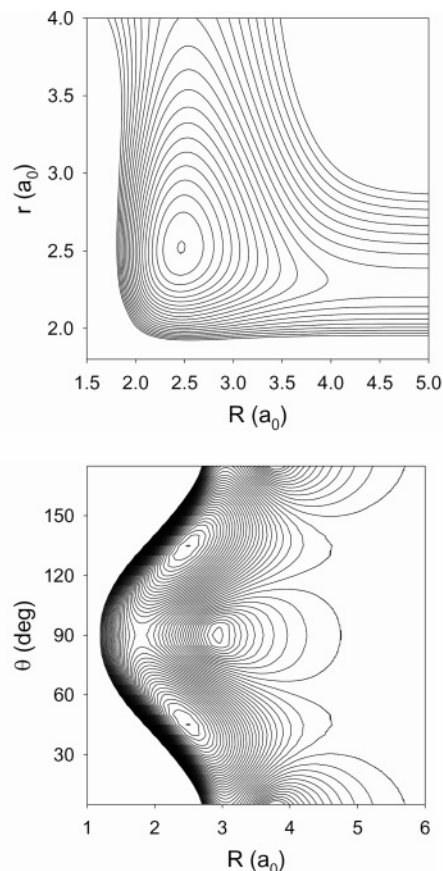


Figure 1. Contours for the Xu, Xie, Zhang, Lin, and Guo (XXZLG) potential energy surface (PES) in Jacobi coordinates with θ fixed at the HO₂ equilibrium value (upper panel) and r fixed at the equilibrium value (lower panel). The contour intervals are 0.2 and 0.1 eV for the upper and lower panels, respectively.

levels, a much smaller grid is sufficient. The converged vibrational energy levels were generated by performing $\sim 30\,000$ Lanczos recursion steps with a cutoff of 6.0 eV for the potential and kinetic energy operators. Test calculations with different DVR grid points were performed to ensure that most of the vibrational energy levels are converged to better than 0.1 cm^{-1} .

A total of 307 bound states were observed to lie below the H + O₂ ($v = 0$, $j = 1$) dissociation limit. The full list of these energy levels is given in Tables 1 and 2. The energy zero is placed at the ground vibrational state, which is 2987.25 cm^{-1} above the potential minimum. In Figure 2, we display the sum of bound states versus energy for both the DMBE IV and modified XXZLG PESs. Clearly, there are much less bound states on the XXZLG PES, rendering a smaller density of states and less opportunities for intermodal coupling.

Low-lying levels have been assigned with the three vibrational quantum numbers, corresponding to the O–H stretch, the H–O–O bend, and the O–O stretch, respectively. The three fundamental frequencies are 3433.03 , 1388.77 , and 1089.95 cm^{-1} , which are very close to the corresponding experimental values (3436.2 , 1391.8 , and 1097.6 cm^{-1}). On the other hand, the corresponding frequencies on the DMBE IV PES (3333.65 , 1296.37 , and 1065.46 cm^{-1})¹⁰ all underestimate the experimental values significantly. The assignment was relatively straightforward, up to $\sim 10\,000\text{ cm}^{-1}$, as shown in Table 1.

However, it becomes more and more difficult to assign the vibrational levels with the increase in energy. The wavefunctions become increasingly irregular, because of intermodal couplings and an increasing density of states. As a result, not all energy levels in Table 2 are assigned. Nevertheless, there are several

TABLE 1: Comparison of Calculated Low-Lying Energy Levels of HO₂ with Those from Different Spectroscopic Hamiltonians and from Available Experimental Band Origins

$n_1 n_2 n_3$	Energy Level (cm ⁻¹)					experiment ^a
	exact	fit with diagonal and off-diagonal terms	difference (rms = 2.1)	fit with diagonal terms	difference (rms = 4.4)	
0 0 0	0.00	0.00	0.00	0.00	0.00	
0 0 1	1089.95	1090.20	-0.25	1091.86	-1.91	1097.6
0 1 0	1388.77	1388.70	0.070	1389.47	-0.70	1391.8
0 0 2	2161.99	2162.47	-0.48	2164.48	-2.49	
0 1 1	2461.88	2461.32	0.56	2462.37	-0.49	
0 2 0	2751.13	2751.77	-0.64	2752.87	-1.74	
0 0 3	3215.60	3216.35	-0.75	3217.79	-2.19	
1 0 0	3433.03	3430.88	2.15	3426.18	6.85	3436.2
0 1 2	3518.06	3517.52	0.54	3517.21	0.85	
0 2 1	3807.51	3806.87	0.64	3807.20	0.31	
0 3 0	4088.58	4089.56	-0.98	4090.67	-2.09	
0 0 4	4250.61	4251.37	-0.76	4251.71	-1.10	
1 0 1	4515.51	4515.13	0.38	4518.93	-3.42	
0 1 3	4557.87	4558.72	-0.85	4553.90	3.97	
1 1 0	4796.43	4796.59	-0.16	4796.45	-0.02	
0 2 2	4848.55	4847.61	0.94	4844.63	3.92	
0 3 1	5127.47	5127.21	0.26	5126.80	0.67	
0 0 5	5266.66	5267.06	-0.40	5266.15	0.51	
0 4 0	5402.07	5402.41	-0.34	5403.33	-1.26	
0 1 4	5565.15	5563.31	1.84	5572.37	-7.22	
1 0 2	5594.55	5598.73	-4.18	5590.68	3.87	
1 1 1	5849.68	5848.69	0.99	5864.34	-14.7	
0 2 3	5880.55	5880.74	-0.19	5865.08	15.5	
1 2 0	6125.98	6129.23	-3.25	6134.96	-8.98	
0 3 2	6155.94	6154.86	1.08	6147.20	8.74	
0 0 6	6263.07	6262.95	0.12	6261.04	2.03	
0 4 1	6422.53	6422.67	-0.14	6421.64	0.89	
0 1 5	6570.78	6570.11	0.67	6572.53	-1.75	
2 0 0	6633.72	6636.02	-2.30	6637.38	-3.66	6651.19
1 0 3	6645.98	6641.93	4.05	6641.35	4.63	
0 5 0	6691.74	6690.68	1.06	6691.31	0.43	
0 2 4	6864.34	6862.95	1.39	6868.47	-4.13	
1 1 2	6916.78	6916.69	0.09	6912.40	4.38	
0 3 3	7144.98	7145.50	-0.52	7151.78	-6.80	
1 2 1	7184.91	7183.72	1.19	7178.37	6.54	
0 0 7	7239.35	7238.59	0.76	7236.30	3.05	
0 4 2	7418.53	7422.24	-3.71	7425.37	-6.84	
1 3 0	7446.82	7446.49	0.33	7442.17	4.65	
0 1 6	7553.00	7553.98	-0.98	7554.30	-1.30	
1 0 4	7665.02	7668.93	-3.91	7670.87	-5.85	
0 5 1	7692.79	7693.61	-0.82	7692.16	0.63	
2 0 1	7720.86	7720.34	0.52	7720.33	0.53	
0 2 5	7853.23	7852.54	0.69	7854.71	-1.48	
1 1 3	7942.07	7941.67	0.40	7940.55	1.52	
0 6 0	7956.60	7954.70	1.90	7955.06	1.54	
2 1 0	7985.87	7981.83	4.04	7980.95	4.92	
0 3 4	8138.86	8137.36	1.50	8140.46	-1.60	
0 0 8	8195.31	8193.49	1.82	8191.85	3.46	
1 2 2	8206.25	8204.28	1.97	8203.11	3.14	
0 4 3	8411.46	8412.26	-0.80	8414.46	-3.00	
1 3 1	8462.48	8461.62	0.86	8461.46	1.02	
0 1 7	8514.51	8517.75	-3.24	8517.60	-3.09	
1 0 5	8675.17	8675.98	-0.81	8679.15	-3.98	
0 5 2	8676.99	8680.00	-3.01	8679.61	-2.62	
1 4 0	8719.43	8718.81	0.62	8718.53	0.90	
2 0 2	8779.22	8782.12	-2.90	8780.51	-1.29	
0 2 6	8822.94	8823.46	-0.52	8823.73	-0.79	
0 6 1	8938.17	8940.36	-2.19	8938.84	-0.67	
1 1 4	8950.40	8949.86	0.54	8948.70	1.70	
2 1 1	9033.45	9033.22	0.23	9033.12	0.33	
0 3 5	9115.11	9111.64	3.47	9113.16	1.95	
0 0 9	9130.33	9127.20	3.13	9127.61	2.72	
0 7 0	9196.57	9194.81	1.76	9195.05	1.52	
1 2 3	9210.87	9209.57	1.30	9209.10	1.77	
2 2 0	9288.09	9291.59	-3.50	9287.05	1.04	

TABLE 1 (continued)

$n_1 n_2 n_3$	Energy Level (cm ⁻¹)					experiment
	exact	fit with diagonal and off-diagonal terms	difference (rms = 2.1)	fit with diagonal terms	difference (rms = 4.4)	
0 4 4	9390.96	9387.06	3.90	9388.81	2.15	
0 1 8	9455.29	9461.45	-6.16	9462.36	-7.07	
1 3 2	9461.15	9461.72	-0.57	9463.26	-2.11	
3 0 0	9610.41	9610.13	0.28	9610.41	0.00	
0 5 3	9653.26	9652.99	0.27	9653.57	-0.31	
1 0 6	9665.26	9662.10	3.16	9666.11	-0.85	
1 4 1	9708.77	9711.13	-2.36	9714.09	-5.32	
0 2 7	9770.21	9772.71	-2.50	9775.45	-5.24	
2 0 3	9823.30	9822.90	0.40	9817.84	5.46	
0 6 2	9908.93	9911.49	-2.56	9910.38	-1.45	
1 1 5	9939.26	9941.33	-2.07	9936.78	2.48	
1 5 0	9965.57	9963.54	2.03	9964.51	1.06	
2 1 2	10056.4	10056.6	-0.19	10063.7	-7.32	
0 3 6	10081.8	10074.7	7.14	10069.8	12.0	
1 2 4	10197.0	10199.3	-2.33	10196.3	0.68	

^a The experimental references are given in ref 21.

TABLE 2: Energies of Higher Vibrational Levels Not Included in Table 1^a

$n_1 n_2 n_3$	E	$n_1 n_2 n_3$	E	$n_1 n_2 n_3$	E	$n_1 n_2 n_3$	E	$n_1 n_2 n_3$	E	$n_1 n_2 n_3$	E
0 0 10	10043.1	1 1 7	11826.7	1 6 2	13049.6	0 2 12	14161.4		15049.1		15823.0
0 7 1	10160.0	0 6 4	11833.6	2 1 5	13083.9		14178.7		15061.8		15856.0
2 2 1	10303.0	1 5 2	11865.9	0 4 8	13158.8	0 8 4	14184.5		15067.4		15861.7
0 4 5	10358.3	2 0 5	11875.0	3 2 1	13176.1		14222.5	0 12 0	15093.6		15883.8
0 1 9	10375.3	0 3 8	11942.9	2 2 4	13228.9	0 0 15	14224.3		15101.9		15936.1
0 8 0	10411.3	3 1 1	11959.3	1 3 6	13251.4		14238.4		15132.9		15939.5
1 3 3	10441.8	1 2 6	12062.9	0 8 3	13272.3		14328.3		15167.1		15961.6
2 3 0	10556.9	0 7 3	12073.1	1 7 1	13296.6		14345.4		15210.2		15971.5
0 5 4	10621.8	1 6 1	12099.4	0 2 11	13327.1	1 0 11	14349.4	1 0 12	15233.8		16013.2
1 0 7	10631.5	2 1 4	12120.1	4 0 1	13359.5		14358.0		15268.4		16022.1
3 0 1	10670.1	0 1 11	12147.6		13413.9		14386.4		15283.1		16045.1
1 4 2	10684.0	3 2 0	12189.2	0 0 14	13426.4		14415.1		15298.1		16048.9
0 2 8	10704.5	0 4 7	12236.0	0 5 7	13439.7		14433.5		15305.5		16072.0
2 0 4	10844.6	2 2 3	12286.2		13455.1		14448.9	2 6 1	15330.3		16095.0
0 6 3	10872.6	0 8 2	12308.1		13475.5		14476.8		15348.7		16108.9
1 1 6	10907.3	4 0 0	12337.3	0 9 2	13480.1		14550.0		15372.3		16120.9
1 5 1	10913.9	1 3 5	12355.7	2 3 3	13516.7		14588.6	0 1 15	15374.7		16168.0
0 0 11	10932.8	1 7 0	12372.7	1 8 0	13544.7		14595.4		15396.9		16174.4
3 1 0	10944.0	0 2 10	12461.9	0 3 10	13623.5	0 1 14	14601.2		15470.1		16195.3
0 3 7	11012.3	2 3 2	12490.1	3 3 0	13637.6		14623.1		15482.0		16202.9
2 1 3	11081.0	0 5 6	12526.9	1 5 4	13683.8		14635.3		15506.4		16212.1
0 7 2	11118.8	0 9 1	12543.1	0 6 6	13695.4		14658.0		15522.6		16233.9
1 2 5	11164.4	1 0 9	12545.5	0 10 1	13707.1	1 1 10	14665.7	1 1 11	15535.2		16255.1
1 6 0	11182.0	1 4 4	12582.7	3 0 4	13730.7		14702.3		15557.3		16288.5
0 1 10	11272.8	0 0 13	12637.7		13746.3		14709.1		15585.5		16309.7
2 2 2	11288.6	2 4 1	12729.5		13763.9		14722.8		15594.3		16329.7
0 4 6	11321.8	3 0 3	12731.3	0 1 13	13817.5		14756.3		15605.1		16352.9
0 8 1	11360.9	1 1 8	12747.3	2 0 7	13847.5		14824.9		15637.5		16358.7
1 3 4	11405.3	0 10 0	12770.6	0 4 9	13898.2		14832.2		15665.1		16401.1
2 3 1	11532.0	0 6 5	12778.1		13914.2	0 11 1	14839.6		15701.9	0 0 18	16402.2
1 0 8	11566.1	1 5 3	12810.6	0 11 0	13923.5		14848.3	0 0 17	15702.7		16408.9
0 5 5	11581.8	0 3 9	12849.4	0 7 5	13931.2		14894.6		15739.9		16416.1
0 9 0	11601.7	2 0 6	12875.9	3 2 3	13949.3		14905.1		15744.1		16435.6
0 2 9	11627.7	3 1 2	12956.6	1 7 2	13980.4		14948.2	0 2 14	15747.8		16460.7
1 4 3	11636.5	0 1 12	12989.8	1 2 8	14036.7	0 2 13	14950.7		15775.6		16487.1
3 0 2	11715.9	1 2 7	12995.1		14071.3		14961.2		15799.3		16495.3
0 0 12	11792.1	2 5 0	13004.3		14130.6	0 0 16	14979.7		15808.6		16505.8
2 4 0	11796.4	0 7 4	13018.5		14146.2		14996.0		15819.6		

^a The tentative assignment is also included.

high-energy levels that remain regular, even near the dissociation limit. The most conspicuous are the O–O overtones, with up to 18 quanta. The eigenfunctions of the six highest O–O overtones displayed in Figure 3 show clear nodal structures and are readily assignable. This surprising mode-specific feature of HO₂ will be explained with the PO analysis below. We note in

passing that the regularity of the O–O stretching mode has also been noted on the DMBE IV PES,¹⁰ but the overtone is observed only up to $n_3 = 11$.⁸

Interestingly, the highest O–H overtone is the (4,0,0) state, which is located 12337.25 cm⁻¹ above the ground vibrational state. No higher O–H overtone was observed. This observation

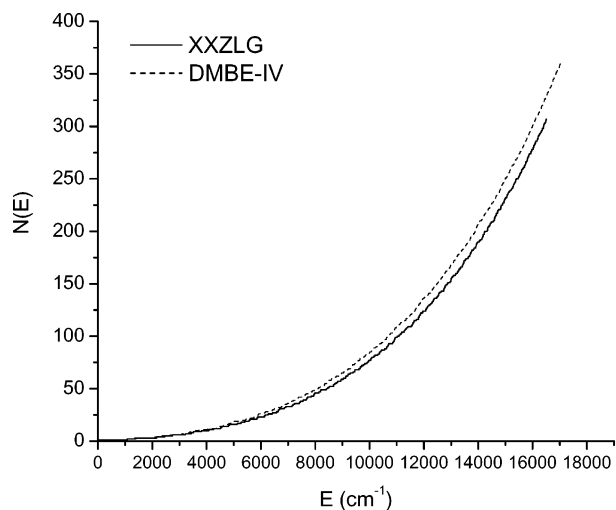


Figure 2. Number of states ($N(E)$) versus energy (E) for both the modified XXZLG and double many-body expansion (DMBE) IV PESs.

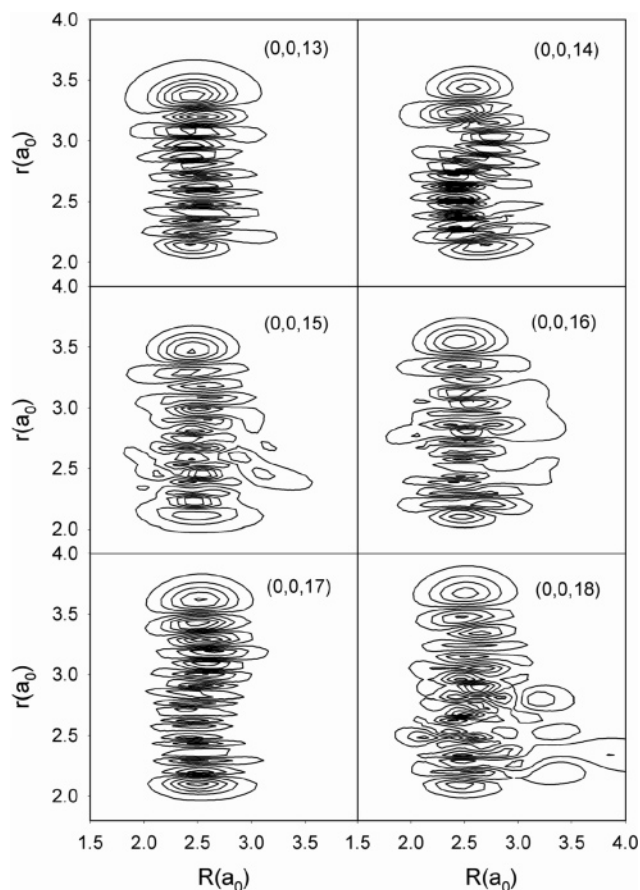


Figure 3. Wavefunctions of highly excited O–O stretching overtones on the modified XXZLG PES.

highlights the floppy nature of the O–H bond in this system. As the contour plot of the PES in the (R, θ) coordinates (Figure 1, lower panel) shows, a barrier exists between two isomers of HO_2 . The isomerization barrier is ~ 1.6 eV above the potential minimum, which is approximately the energy of the $(4,0,0)$ state. Above this barrier, the coupling between the O–H stretch and the H–O–O bend is expected to be very strong, which may destroy the mode specificity in the OH stretch.

The coexistence of regular and irregular energy levels in the same energy region is confirmed by the NNLS and Δ_3 distributions in Figure 4. It is readily observed from the figure

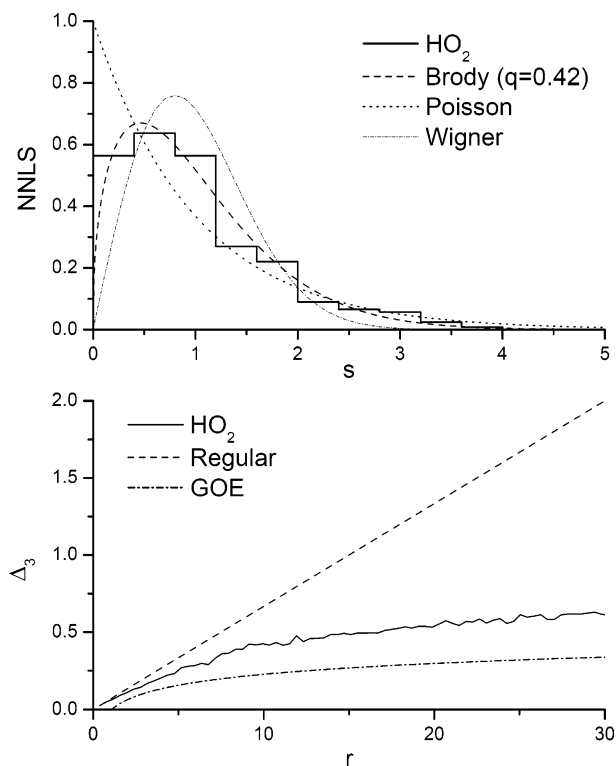


Figure 4. Nearest-neighbor-level spacing (NNLS) and Δ_3 distributions for the HO_2 vibrational levels. In the NNLS distribution, the regular and chaotic limits are represented by the Poisson and Wigner distributions. The chaotic limit is given by the Gaussian Orthogonal Ensemble (GOE) for the Δ_3 distributions.

that the NNLS distribution is neither Wigner nor Poisson, which represent the chaotic and regular limits, respectively. It is interesting to note the depletion of the NNLS distribution at small values of s , which is indicative of significant interactions between nearest neighbors. The distribution is best-fit by the Brody distribution⁵² with $q = 0.47$. Similarly, the Δ_3 distribution is located between the regular limit and the Gaussian Orthogonal Ensemble (GOE) limit, indicating a mixture of regular and irregular states. These results, which has been reported earlier in our preliminary report,²³ are in sharp contrast to the earlier conclusion based on the DMBE IV PES that the HO_2 vibration is purely chaotic.²⁰ It is likely that the chaotic vibrational spectrum on the DMBE IV PES stems from the underestimation of the HO_2 fundamental frequencies, which results in an overestimation of the state density.

The increasing irregularity of the highly excited eigenfunctions can be attributed to intermodal couplings embedded in the anharmonic PES. Such couplings manifest in terms of Fermi resonances, which convolute the nodal structures in the eigenfunctions by mixing zeroth-order states. The most-prominent Fermi resonances are usually among those zeroth-order states with close energies. We have identified several important Fermi resonances in the HO_2 spectrum. For instance, the 1:1+2 resonance corresponds to the annihilation of one quantum in the O–H stretch and the creation of one quantum in the H–O–O bend and two quanta in the O–O stretch, or vice versa. This resonance is apparently dictated by the frequencies of three vibrational modes, namely, $\omega_1 \approx \omega_2 + 2\omega_3$. This resonance emerges quite early in the energy spectrum. A prime example is the $(1,1,1)/(0,2,3)$ pair, which is plotted in Figure 5. The two eigenvalues differ only by 30.87 cm^{-1} and the shapes of the wavefunctions are quite similar. In the same figure, the zeroth-order wavefunctions, which are recovered from the eigenfunc-

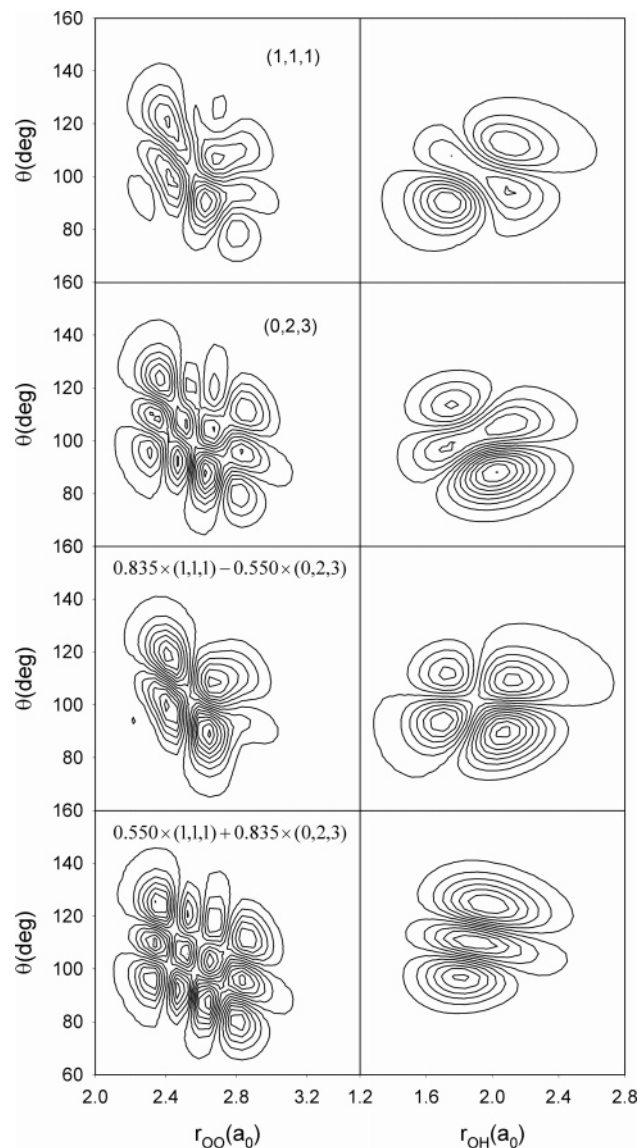


Figure 5. Wavefunctions for the (1,1,1) and (0,2,3) states and their linear combinations.

tions by linear combination, are also presented, and the nodal structures are much clearer and consistent with the assignments.

Other low-lying Fermi-type resonances include 2:2+4 and 4:5 resonances, as exemplified by the (2,1,2)/(0,3,6) pair and the (1,1,6)/(1,5,1) pair, respectively. These two resonances are in higher order than the 1:1+2 resonance mentioned above and occur at higher energies.

To further understand the spectrum, we fit the 80 lowest-lying energy levels to a spectroscopic Hamiltonian. We found it difficult to fit the spectrum well with the diagonal Hamiltonian in eq 7 alone, because of the prominent 1:1+2 resonance. The root-mean-square (rms) error for such a fit was 4.4 cm⁻¹, and the energy levels affected by the resonance are particularly difficult to fit, as shown in Table 1. As a result, we included in the fitting the off-diagonal term described by eq 8, which represents the contribution of the 1:1+2 resonance. The fit improved, reducing the rms error to 2.1 cm⁻¹. The resulting spectroscopic constants are shown in Table 3, and the energy levels calculated from the model Hamiltonian are compared to the exact values in Table 1. The other two resonances were not considered, because they appear at relatively high energies. Overall, the HO₂ spectrum is not strongly affected by these resonances.

TABLE 3: Parameters of the Spectroscopic Hamiltonian

parameter	fit (cm ⁻¹)
ω_1	3663.14750
ω_2	1430.88235
ω_3	1116.31814
x_{11}	-110.56538
x_{21}	-14.49079
x_{22}	-11.79833
x_{31}	0.96499
x_{32}	-15.07537
x_{33}	-8.49613
y_{111}	-0.72551
y_{211}	0.64014
y_{221}	-2.57525
y_{222}	0.05741
y_{311}	0.50659
y_{321}	-6.87532
y_{322}	0.03094
y_{331}	-0.67106
y_{332}	0.43688
y_{333}	-0.07782
k	11.14220
λ_1	-1.05405
λ_2	0.97161
λ_3	0.40211

The results of our PO analysis are presented in Figure 6 as a continuation/bifurcation diagram. What we have plotted are the frequencies obtained from the periods of POs, as functions of the total energy. The zero energy is the absolute minimum of the potential. These frequencies are compared to the energy differences of adjacent vibrational levels for the three overtone series of the molecule (point symbols). The eigenfunctions of the plotted states have clear nodal structures, as discussed previously; therefore, they could easily be assigned. The quantum energy levels have been translated by shifting the zero point energy (ZPE) to the classical zero energy. The principal families of POs are denoted by OH, OO, and B for the O–H stretch, the O–O stretch, and the bend, respectively. SN1 is a new family of POs that emanates from a SN bifurcation of the OO family. As energy increases, the new family also bifurcates and the SN2 POs appear. This scenario of cascading SN bifurcations has been observed and discussed for several molecules.⁵³

In Figure 7, representative POs are shown projected on the (R, r) plane. The three orbits of the O–O stretch demonstrate how the topology changes from energies below the SN1 bifurcation and above. At an energy of ~ 1.5 eV, the family SN1 appears, as a result of the interaction with the O–H stretch. Indeed, in Figure 7, we can see that a 1:4 resonance between

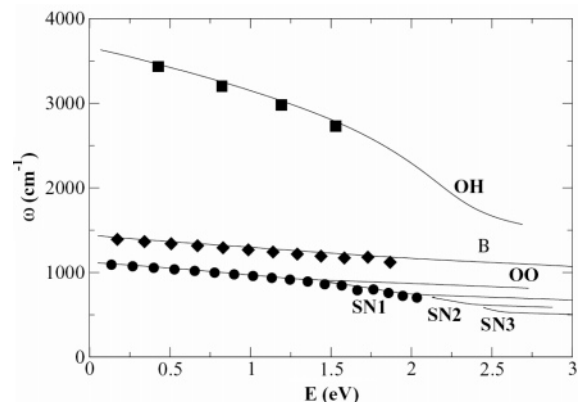


Figure 6. Continuation/bifurcation diagram of HO₂. OH, OO, and B denote the O–H stretching, O–O stretching, and bending modes, respectively. SN denotes saddle-node bifurcation.

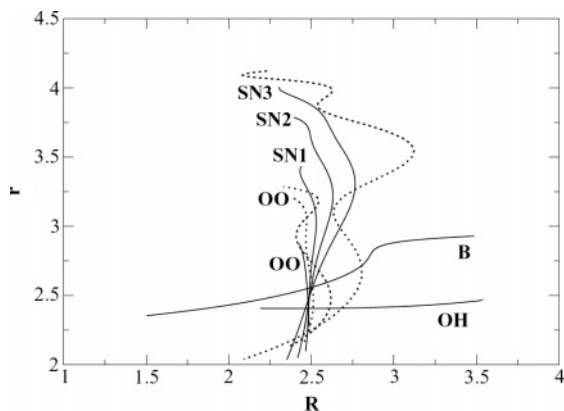


Figure 7. Plots of representative periodic orbits (POs). Distances are given in atomic units and energies are given in electron volts: OO at energies of 0.47 (solid), 1.17 (dotted), 1.47 (dotted); SN1 at energies of 1.66, SN2 2.21, SN3 2.47 (solid) 3.02 (dotted); OH at an energy of 2.15; and B at an energy of 2.97.

the two stretches has been developed for the OO PO (dotted curves). As the energy increases, higher resonances between the OO and OH result in new bifurcations, whereas the frequency of the parent family levels off. From the plot of the SN3 PO (dotted curve), we can see that a 1:7 resonance has been developed. Because of these resonances, energy is pumped into the OH stretching mode and not in the OO stretching mode. Initially, the newborn family carries the same morphology as the parent family. The POs are stable and, thus, the localization of eigenfunctions can be justified. The stable branch of the SN2 and SN3 covers smaller energy intervals and it is likely they cannot support more-localized quantum states.

The morphologies of the OH and B families remain the same for the entire energy range. Examples for the OH and B POs are shown in Figure 7 at energies of 2.15 and 2.97 eV, respectively. The OH family turns to single unstable at ~ 1.3 eV, whereas it becomes a complex unstable at 1.8 eV. Above these energies, the anharmonicity of the OH mode increases substantially, as can be observed in Figure 6. Thus, the instability developed in this region of phase space is in accord with our difficulties in assigning higher quantum OH states. The B family becomes single unstable at 2.4 eV, after a period-doubling bifurcation. We have no clearly assigned bend states above this energy; therefore, we have not searched for the bifurcating half-frequency POs. However, the strong coupling between the OH stretching and bending modes is apparent in the representative B family PO in Figure 7.

Although the stability of POs provides information about near-neighboring trajectories, the existence of stable POs at high energies reveal the mixed character of phase space (regular/chaotic), in good agreement with the observations from the NNLS and Δ_3 distributions. In particular, our PO analysis provides additional evidence in support of the conclusion that the OO stretch possesses regularity all the way to the dissociation limit.

IV. Conclusions

In this publication, we have provided a thorough analysis of the vibrational spectrum and dynamics of the HO₂ system, based on a new and accurate potential energy surface (PES). It is shown that the vibration of HO₂ is quite regular at low energies, but increased irregularity at higher energies prevents the assignment of all vibrational levels. Overall, the vibrational spectrum can be considered as an intermediate case with mixed regularity and irregularity. An interesting observation is the

regularity in the OO stretch overtones up to the H + O₂ asymptote, which is due to the emergence of saddle-node (SN) bifurcations. This conclusion is in contrast to that obtained earlier on the semiempirical double many-body expansion (DMBE) IV PES, which showed complete chaotic vibration at high energies.²⁰

It is not yet clear how the difference in the PESs will impact the dynamics of both unimolecular reactions (reaction R2) and bimolecular reactions (reactions R1 and R3). Our recent results at $J = 0$ have demonstrated substantial changes in the reaction probability for reaction R1.²⁴ However, the large exothermicity and dominance of long-range electrostatic interactions in the HO + O channel in the reactivity of reaction R1 may render averaged reaction attributes, such as cross sections and rate constant, insensitive to the details of the PES in the strongly interacting regions. On the other hand, we expect that the unimolecular decay of the HO₂ species will be strongly affected by the weak intermodal coupling and lower density of states. More studies on resonance lifetimes of HO₂ are needed.

Acknowledgment. This research was in parts supported by the National Natural Science Foundation of China (Grant Nos. 10574068 and 20533060 to author D.X.), by an EU ToK grant (No. MTKD-CT-2005-029583 to author S.C.F.), and by the National Science Foundation (CHE-0348858 to author H.G.). Author H.G. would also like to thank Michael Kellman for several useful discussions.

References and Notes

- (1) Miller, J. A.; Kee, R. J.; Westbrook, C. K. *Annu. Rev. Phys. Chem.* **1990**, *41*, 345.
- (2) Smith, I. W. M.; Herbst, E.; Chang, Q. *Mon. Not. R. Astron. Soc.* **2004**, *350*, 323.
- (3) Troe, J. *Chem. Rev.* **2003**, *103*, 4565.
- (4) Summers, M. E.; Conway, R. R.; Siskind, D. E.; Stevens, M. H.; Offermann, D.; Riese, M.; Preusse, P.; Strobel, D. F.; Russell, J. M. *Science* **1997**, *277*, 1967.
- (5) Miller, J. A.; Pilling, M. J.; Troe, J. *Proc. Combust. Inst.* **2005**, *30*, 43.
- (6) Pastrana, M. R.; Quintales, L. A. M.; Brandao, J.; Varandas, A. J. *C. J. Phys. Chem.* **1990**, *94*, 8073.
- (7) Zhang, D. H.; Zhang, J. Z. H. *J. Chem. Phys.* **1994**, *101*, 3671.
- (8) Dobbyn, A.; Stumpf, M.; Keller, H.-M.; Schinke, R. *J. Chem. Phys.* **1995**, *103*, 9947.
- (9) Dobbyn, A.; Stumpf, M.; Keller, H.-M.; Schinke, R. *J. Chem. Phys.* **1996**, *104*, 8357.
- (10) Mandelshtam, V. A.; Grozdanov, T. P.; Taylor, H. S. *J. Chem. Phys.* **1995**, *103*, 10074.
- (11) Chen, R.; Guo, H. *Chem. Phys. Lett.* **1997**, *277*, 191.
- (12) Wu, X. T.; Hayes, E. F. *J. Chem. Phys.* **1997**, *107*, 2705.
- (13) Zhang, H.; Smith, S. C. *J. Chem. Phys.* **2003**, *118*, 10042.
- (14) Zhang, H.; Smith, S. C. *J. Chem. Phys.* **2004**, *120*, 9583.
- (15) Zhang, H.; Smith, S. C. *J. Chem. Phys.* **2005**, *123*, 014308.
- (16) Kendrick, B.; Pack, R. T. *J. Chem. Phys.* **1995**, *102*, 1994.
- (17) Harding, L. B.; Maergoiz, A. I.; Troe, J.; Ushakov, V. G. *J. Chem. Phys.* **2000**, *113*, 11019.
- (18) Troe, J.; Ushakov, V. G. *J. Chem. Phys.* **2001**, *115*, 3621.
- (19) Varandas, A. J. C.; Brandao, J.; Pastrana, M. R. *J. Chem. Phys.* **1992**, *96*, 5137.
- (20) Schinke, R.; Keller, H.-M.; Flothmann, H.; Stumpf, M.; Beck, C.; Mordaunt, D. H.; Dobbyn, A. J. *Adv. Chem. Phys.* **1997**, *101*, 745.
- (21) Xu, C.; Xie, D.; Zhang, D. H.; Lin, S. Y.; Guo, H. *J. Chem. Phys.* **2005**, *122*, 244305.
- (22) Xie, D.; Xu, C.; Ho, T.-S.; Rabitz, H.; Lendvay, G.; Lin, S. Y.; Guo, H. *J. Chem. Phys.* **2007**, *126*, 074315.
- (23) Lin, S. Y.; Xie, D.; Guo, H. *J. Chem. Phys.* **2006**, *125*, 091103.
- (24) Lin, S. Y.; Guo, H.; Honvault, P.; Xie, D. *J. Phys. Chem. B* **2006**, *110*, 23641.
- (25) Golub, G. H.; Van Loan, C. F. *Matrix Computations*, 3rd Edition; The Johns Hopkins University Press: Baltimore, MD, 1996.
- (26) Parlett, B. N. *The Symmetric Eigenvalue Problem*; Prentice Hall: Englewood Cliffs, NJ, 1980.
- (27) Lanczos, C. *J. Res. Natl. Bur. Stand.* **1950**, *45*, 255.
- (28) Nauts, A.; Wyatt, R. E. *Phys. Rev. Lett.* **1983**, *51*, 2238.

- (29) Wyatt, R. E.; Scott, D. S. Quantum dynamics with the recursive residue generation method: Improved algorithm for chain propagation. In *Large Scale Eigenvalue Problems*; Cullum, J., Willoughby, R. A., Eds.; North Holland: Amsterdam, 1986; pp 67.
- (30) Wyatt, R. E. *Adv. Chem. Phys.* **1989**, *73*, 231.
- (31) Carrington, T., Jr. *Can. J. Chem.* **2004**, *82*, 900.
- (32) Guo, H. *Rev. Comput. Chem.* in press.
- (33) Cullum, J. K.; Willoughby, R. A. *Lanczos Algorithms for Large Symmetric Eigenvalue Computations*; Birkhauser: Boston, 1985; Vol. I.
- (34) Guo, H.; Chen, R.; Xie, D. *J. Theor. Comput. Chem.* **2002**, *1*, 173.
- (35) Light, J. C.; Carrington, T., Jr. *Adv. Chem. Phys.* **2000**, *114*, 263.
- (36) Colbert, D. T.; Miller, W. H. *J. Chem. Phys.* **1992**, *96*, 1982.
- (37) Light, J. C.; Hamilton, I. P.; Lill, J. V. *J. Chem. Phys.* **1985**, *82*, 1400.
- (38) Chen, R.; Guo, H. *Chem. Phys. Lett.* **1999**, *308*, 123.
- (39) Kellman, M. E. *Annu. Rev. Phys. Chem.* **1995**, *46*, 395.
- (40) Vanderplaats, G. N. *Numerical Optimization Techniques for Engineering Design*; McGraw-Hill: New York, 1984.
- (41) Wigner, E. P. *SIAM Rev.* **1967**, *1*, 1.
- (42) Dyson, F. J.; Mehta, M. L. *J. Math. Phys.* **1963**, *4*, 701.
- (43) Zimmerman, T.; Cederbaum, L. S.; Meyer, H.-D.; Köppel, H. *J. Phys. Chem.* **1987**, *91*, 4446.
- (44) Ishikawa, H.; Field, R. W.; Farantos, S. C.; Joyeux, M.; Koput, J.; Beck, C.; Schinke, R. *Annu. Rev. Phys. Chem.* **1999**, *50*, 443.
- (45) Joyeux, M.; Farantos, S. C.; Schinke, R. *J. Phys. Chem.* **2002**, *106*, 5407.
- (46) Joyeux, M.; Grebenshchikov, S. Y.; Bredenbeck, J.; Schinke, R.; Farantos, S. C. *Adv. Chem. Phys.* **2005**, *130*, 267.
- (47) Farantos, S. C.; Lin, S. Y.; Guo, H. *Chem. Phys. Lett.* **2004**, *399*, 260.
- (48) Lin, S. Y.; Guo, H.; Farantos, S. C. *J. Chem. Phys.* **2005**, *122*, 124308.
- (49) Hanssmann, H. *Local and Semi-Local Bifurcations in Hamiltonian Dynamical Systems, Lecture Notes in Mathematics*; Springer-Verlag: Berlin, 2007.
- (50) Farantos, S. C. *THEOCHEM, J. Mol. Struct.* **1995**, *341*, 91.
- (51) Farantos, S. C. *Comput. Phys. Commun.* **1998**, *108*, 240.
- (52) Brody, T. A.; Flores, J.; French, J. B.; Mello, P. A.; Pandey, A.; Wong, S. S. M. *Rev. Mod. Phys.* **1981**, *53*, 385.
- (53) Farantos, S. C.; Qu, Z.-W.; Zhu, H.; Schinke, R. *Int. J. Bifurcation Chaos Appl. Sci. Eng.* **2006**, *16*, 1913.